analytical chemistry

Article

pubs.acs.org/ac

Surface Enhanced Raman Correlation Spectroscopy of Particles in Solution

Steven M. Asiala and Zachary D. Schultz*

Department of Chemistry and Biochemistry, University of Notre Dame, Notre Dame, Indiana 46556, United States

ABSTRACT: Surface enhanced Raman correlation spectroscopy (SERCS) is shown as a label-free, chemically specific method for monitoring individual polymer beads and lipid vesicles interacting with a 2-D planar surface enhanced Raman (SERS) substrate in solution. The enhancement afforded by the SERS substrate allows for spectral data to be acquired in series at rates between 31 and 83 Hz. Auto- and cross-correlation of spectral data facilitates the measurement of diffusion constants for particles ranging in radius from 50 to 500 nm while discriminating signal associated with the target analyte from extraneous fluctuations. The measured diffusion coefficients are on the order of 10^{-10}–10^{-11} cm^2/s, a factor of 40 times slower than predicted from the Stokes–Einstein equation, suggesting that particles are experiencing hindered diffusion at the surface. The enhanced signals appear to originate from particles less than 5 nm of the SERS substrate, consistent with adsorption to the surface. This work provides a means to measure and monitor surface interactions and demonstrates the utility and limits of SERS detection in solution over planar SERS substrates.

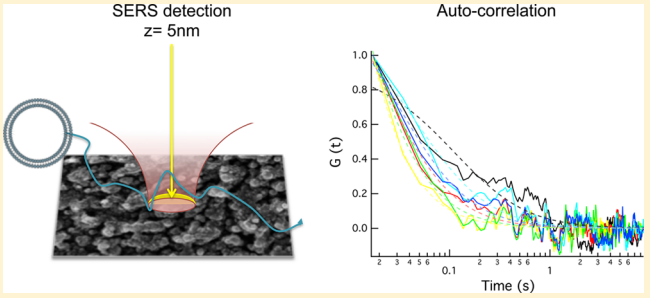

Surface enhanced Raman spectroscopy (SERS) has been repeatedly demonstrated as a powerful tool for ultrasensitive chemical detection.[1−3] Since the initial observation of Raman enhancement on a roughened Ag electrode[4,5] an understanding of the underlying mechanisms that give rise to the observed enhancement has been established. A localized surface plasmon resonance (LSPR) generates an increased electric field and also reradiates Raman scattering.[6] The combination of these effects can generate enhancements up to 10^{11} when optimized,[7] sufficient for the detection of single molecules.[8−11] The formation of chemisorbed adlayers often shows additional enhancement, the so-called chemical enhancement effect, associated with the formation of a surface complex.[12] It is now understood that the largest enhancements arise from metallic junctions consisting of two or more nanostructures in close proximity (1−2 nm), with the greatest field—a SERS "hot spot"—localized at the space between them.[7,13]

Hot spots have been shown to dominate observed SERS signals;[14,15] however, recent studies have suggested that SERS enhancements originating from molecules outside of the junction gap also generate appreciable SERS signals.[16,17] Studies comparing the spatial location of the Rayleigh scattering maximum, or hot spot, with the location of the SERS intensity maximum suggest that enhancement outside of the gap region is sufficient for detection at the single-molecule limit.[16] Further, the finding that the SERS enhancement factor is insensitive to the number of particles in an assembly of nanostructures[15] suggests that perhaps the model in which hot spots dominate the observed SERS spectrum is insufficient to explain the whole picture. In aggregated nanostructured systems with high densities of hotspots, such as our SERS substrate[18] and the randomly arranged surfaces fabricated by Nishijima et al.,[19] the resulting fringing field provides a mechanism for enhancement and detection of molecules outside gap junctions. In our recent communication, we showed that individual polystyrene beads and lipid vesicles could be detected diffusing across a SERS substrate in solution.[17] Clearly, these assemblies are too large to fit inside a 1−2 nm gap between nanostructures.

The field enhancements obtained upon excitation of an LSPR have been shown to decay rapidly from the nanostructure surface.[20,21] Empirical investigations based on molecules confined to the surface show an r^{-10} dependence associated with the nanostructure radius,[20] as well as an exponential decrease associated with the curvature of the surface.[21] In either analysis, the SERS enhancement is reported to be a short-range effect.

In this report, we demonstrate the utility of the large enhancements observed on a planar SERS substrate to facilitate rapid spectral acquisition of particles diffusing in solution. Correlation analysis uses signal intensity fluctuations to gain information related to the size and diffusion dynamics of a species, as well as species concentration. Although dynamic light scattering (DLS)[22] and fluorescence correlation spectroscopy[23] are the most commonly utilized forms of correlation analysis, it has also been demonstrated using Raman spectroscopy (RCS)[24] and SERS[25−27] from nanoparticles and

Received: November 29, 2013
Accepted: February 6, 2014
Published: February 6, 2014

   dx.doi.org/10.1021/ac403882h | *Anal. Chem.* 2014, 86, 2625−2632

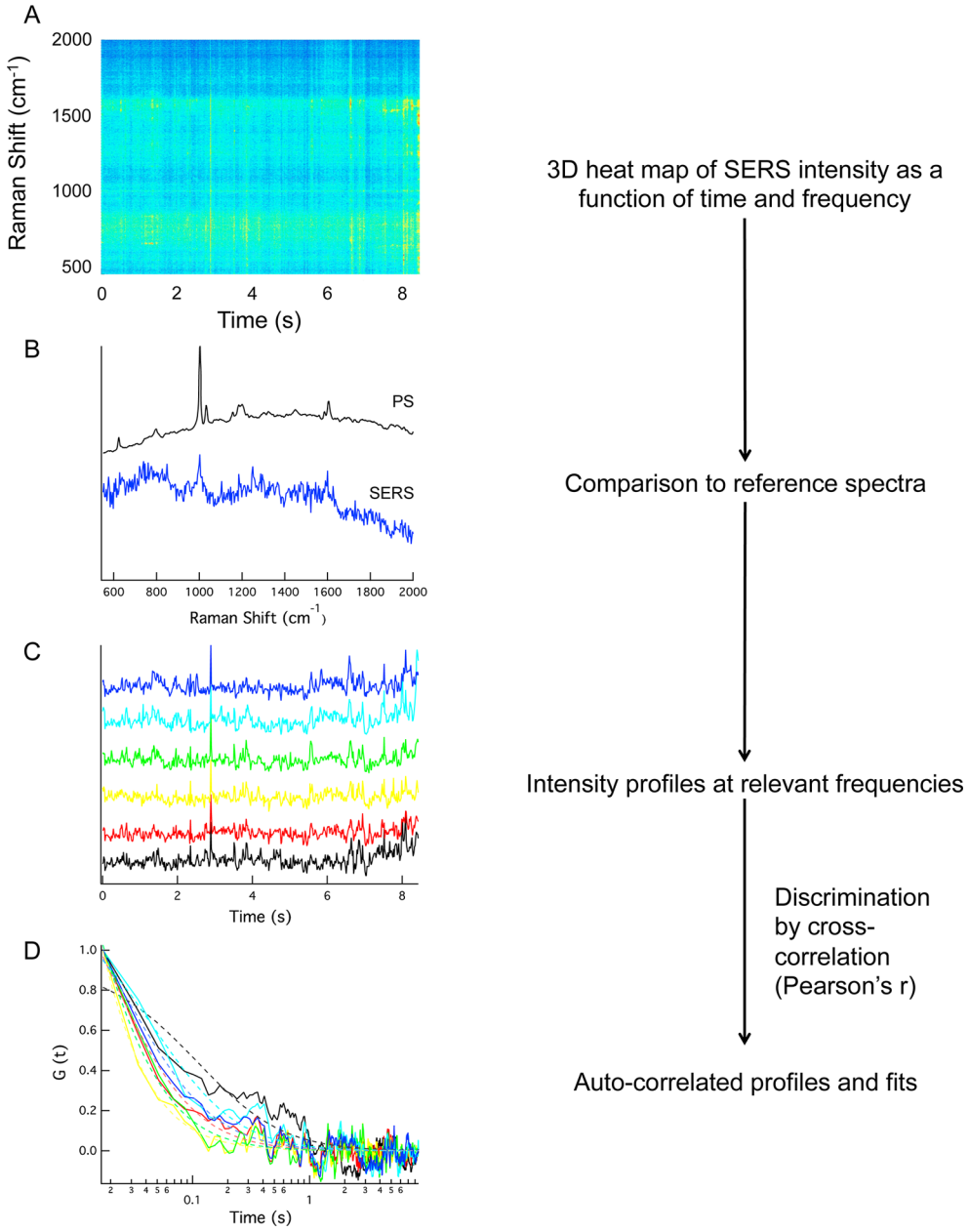

Figure 1. Example of data analysis performed on 10 ms, 440 nm PS bead SERS spectra collected in kinetic series. Panel A shows a 3D heat map of the SERS intensity as a function of time and frequency; B, the spectrum at t = 2.87s (blue) compared with the PS reference spectrum (black); and C plots the intensity vs time profiles at relevant PS frequencies: 627 (black), 1009 (red), 1035 (yellow), 1205 (green), 1498 (light blue), and 1610 cm^{-1} (blue). Panel D shows autocorrelated profiles, which are fit to a model to determine a correlation decay time. From the decay times, the diffusion coefficient can be determined.

aggregates. With the enhancement afforded by our SERS substrate, we are able to collect spectra at a rate sufficient to demonstrate meaningful correlations and fits for lipid vesicles and polymer beads ranging from 100 to 1000 nm in diameter diffusing above an enhancing surface. We demonstrate the utility and limits of surface enhanced Raman correlation spectroscopy (SERCS) as a chemically specific method of monitoring surface interactions in solution.

EXPERIMENTAL SECTION

SERS Measurements. All experiments were performed on a lab-built Raman microscope based on an Olympus BX-51 microscope body.[17,18] Key components include a 17mW HeNe laser (Melles Griot) at 623.8 nm, an OD6 Rugate notch filter (Edmond Optics), and an i303 spectrograph equipped with a Newton 970 EMCCD camera (Andor). The EMCCD camera was binned vertically and operated in electron multiplying mode. Water dipping objectives (Olympus, 40×, 0.8NA and Leica 63×, 0.9NA) were used for excitation and collection of the Raman signal. The collected Raman scattering is focused onto the entrance slit by an f-matched lens (Olympus, 4X, 0.1NA) to maximize the amount of collected scatter onto the EMCCD detector.

SERS substrates were fabricated as described previously.[18] Briefly, silver was vapor-deposited onto a porous anodized aluminum (AAO) substrate with 100 nm pores (Whatman, Anodisc 13). The film was epoxied to a glass slide, and the AAO template was stripped by soaking the substrate for 24 h in

dx.doi.org/10.1021/ac403882h | Anal. Chem. 2014, 86, 2625−2632

0.1 M NaOH (Sigma-Aldrich). The resulting nanostructured silver film SERS substrate has been reported to show an enhancement factor on the order of 10^8.

Spectral data were collected in series at readout rates from 31 to 83 Hz. The series varied in length from 250 to 1000 spectra. The laser power was attenuated to 1 mW with a combination of a half wave plate and polarizer. The temperature was not explicitly controlled, but was monitored to be between 20 and 25 °C, with less than 1 °C variation during experiments. Data analysis was performed in MATLAB (MathWorks). In total, 317 kinetic series were collected and analyzed.

Sample Preparation. Solutions containing 1,2-dipalmityol-*sn*-glycero-3-phosphocholine (DPPC) (Avanti Polar Lipids) single-shell vesicles of varying sizes were prepared by extrusion through polycarbonate filters (Whatman, Nuclepore) with decreasing pore size (1000, 400, 200, and 100 nm).[28] For SERS experiments, vesicle solutions were diluted to 0.05 wt % with nanopure water (18.2 MΩ-cm, Thermo Scientific). Polystyrene beads (Sigma-Aldrich) of varying sizes (1100, 300, and 100 nm) were diluted to 0.001 wt % in nanopure water. A 200 μL drop of diluted solution was placed directly onto the substrate, and meniscus contact was made with the dipping objective.

Dynamic Light Scattering. Samples were independently sized using a Zetasizer Nano ZS (Malvern) with DPPC and PS bead solutions of 0.025 and 0.00025 wt %, respectively. Individual sizing runs consisted of 11 measurements taken in a backscattering configuration. Three sizing runs were averaged to determine the average particle size and standard deviation for each solution.

RESULTS

Polystyrene Beads. Data from a representative kinetic series collection of 0.001 wt % 440 nm PS beads are shown in Figure 1. The collection shown was acquired with 10 ms spectral collection times (10 ms acquisition, 60 Hz) for 500 spectra. The acquisition conditions do not generate measurable spontaneous Raman signal; therefore, all signal measured must arise from SERS.

Figure 1A shows a three-dimensional heat map of SERS signal intensity as a function of both time (x axis) and spectral frequency (y axis). The measured SERS intensity, as a function of the two variables, is represented as a color, with blue representing low intensity and red high intensity. Individual spectra in the kinetic series show bands corresponding to reference spectrum for the given material (Figure 1B). The spectra in Figure 1B are from a polystyrene reference (black) and the spectrum in the heat map at t = 2.87s (blue). The peak intensities observed at 627, 1005, 1200, and 1610 cm^{-1} are indicative of a PS bead near the enhancing surface. These peaks correspond to the ring-stretching (627, 1200, 1610 cm^{-1}) and ring-breathing (1005 cm^{-1}) modes of PS.[29] Also present in the spectrum is a reproducible background signal attributable to the substrate with a pronounced shoulder between 600 and 800 cm^{-1}.

The time-dependent intensity fluctuations associated with peaks in the kinetic series were determined by integrating spectral intensity over a width of ~10 cm^{-1} (5 pixels) around peaks in the reference spectrum, as shown in Figure 1C. The spectra are best characterized as a constant background with intermittent signal bursts attributable to particles moving in and out of the detection area.

Differences in adsorption geometry can lead to the observation of different bands from the same molecule. Further, random intensity fluctuations from impurities or overall changes in background signal can artifactually appear in the intensity profiles. However, Raman spectra are inherently multiplexed in that a single spectrum typically contains multiple peaks attributable to the functional groups present in the sample. To determine if peak fluctuations arise from the same particle, the intensity profiles were subjected to Pearson's r cross-correlation analysis (eq 1).[30]

$$r = \frac{\sum_m \sum_n (A_{mn} - \bar{A})(B_{mn} - \bar{B})}{\sqrt{(\sum_m \sum_n (A_{mn} - \bar{A})^2)}\sqrt{(\sum_m \sum_n (B_{mn} - \bar{B})^2)}} > 0.5 \quad (1)$$

In eq 1, A and B represent the values of two given intensity profiles, and $\bar{A}$ and $\bar{B}$ are the means of those two intensity profiles. The cross-correlation coefficient was used to establish a threshold ($r > 0.5$) to discriminate between Raman band profiles demonstrating statistically significant correlation, or signal, versus those demonstrating uncorrelated or negatively correlated noise.

Figure 1C shows intensity profiles at multiple Raman frequencies present in the PS reference spectrum, including 627 (black), 1009 (red), 1035 (yellow), 1205 (green), 1498 (light blue), and 1610 cm^{-1} (blue). In accordance with what is observed in the spectra in panel B, each profile shows a spike in intensity at t = 2.87s. Profiles showed a strong positive correlation were included in the autocorrelation analysis (Figure 1D).

Profiles with strong positive cross-correlation scores were autocorrelated to generate decay curves. A functional model for three-dimensional diffusion in solution[31] was fit to the resulting autocorrelation curves to establish characteristic decay times (τ_D.)

$$G(t) = \frac{\langle I(t)\, I(t+\tau)\rangle}{\langle I(t)\rangle^2} = \left(\frac{1}{V_{eff}[C]}\right)\left(\frac{1}{1+\frac{t}{\tau_D}}\right)\left(\frac{1}{\sqrt{1+\frac{t}{s^2\tau_D}}}\right) \quad (2)$$

In eq 2, $I(t)$ represents the signal intensity at a give time, $I(t + \tau)$ is the intensity at some time delay (τ) from time t, V_{eff} is the effective focal volume, $[C]$ is the average concentration of the particle, s represents the aspect ratio of the detection volume defined by the axial height of the signal generation area (a) divided by the spot radius (r, $s = a/r$), and τ_D is the characteristic decay time. The decay time can be tied to the diffusion coefficient (D) as shown in eq 3, which, for particles undergoing Brownian motion, can be used to determine the particle radius (r) given the laser beam waist (r_0) through the Stokes–Einstein relation (eq 4).[23,31]

$$\tau_D = \frac{r_0^2}{4D} \quad (3)$$

$$D = \frac{k_B T}{6\pi\eta r} \quad (4)$$

The axial height parameter (a) in eq 2 is often empirically measured in traditional correlation spectroscopy. The unique probe volume associated with SERS requires a modification to commonly used models.[23] Figure 2 depicts differences in the optical geometry between conventional correlation spectrosco-

dx.doi.org/10.1021/ac403882h | Anal. Chem. 2014, 86, 2625–2632

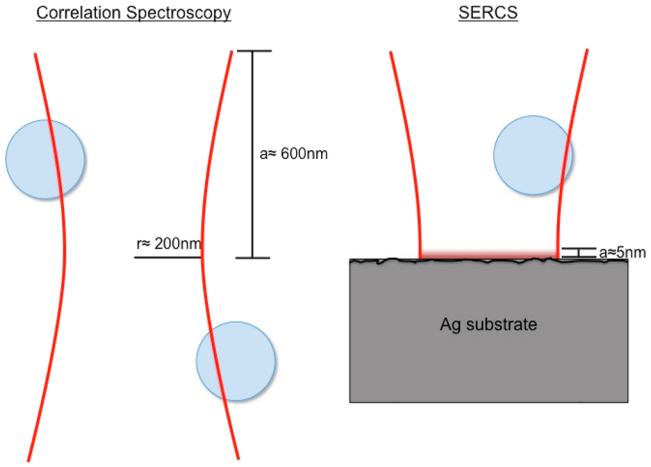

Figure 2. Schematic representation of optical geometries in traditional correlation spectroscopy and SERCS, demonstrating the difference in axial component of the signal generation volume. The red portion in the SERCS image represents the extent of the SERS-enhanced field above the substrate.

py and the experiments described. In traditional correlation spectroscopy, the laser spot radius (r) and the axial depth (a) of the focus define the effective focal volume. These two parameters are combined in the focal volume shape parameter, s, for fitting correlation curves to eq 2.

Given that SERS is a short-range effect (<10 nm),[20,21] it would be inappropriate to approximate the axial depth of the excitation volume as a traditional 2-D Gaussian. The axial depth of the signal-generating region is limited to the extent of propagation of the SERS enhanced field away from the surface. That is, for a given assembly to demonstrate a measurable signal fluctuation, it must approach the surface within the SERS field. It has been demonstrated that the SERS enhancement decays[20] as $1/r^{10}$ or exponentially;[21] however, both of these functions require either knowledge of the nanoparticle radius[20] or the SERS propagation length.[21] To calculate an approximate probe volume, we have simplified the axial height to a fixed value. An approximated axial height of 5 nm was selected for autocorrelation fits in these studies on the basis of the magnitude and frequencies of the SERS signals with different size particles (see below).

Figure 3A shows how the average derived diffusion constant for a sample set of 150 nm DPPC vesicle curves depends upon the height of the probe volume, holding the radial dimension constant. The axial length can be adjusted as a fit parameter in eq 2, and generally, as the axial length is increased, the diffusion constants extracted from the fit increase as shown. The error in choosing a fixed axial height of 5 nm is relatively small over the physically relevant range (Figure 3A inset) of values (0−10 nm) when compared with the errors associated with fits to eq 2 or multiple measurements.

The second fit parameter is the radius of the collection volume. The spot radius in these experiments is best characterized as the diffraction limited spot of the focusing objective. Essentially, there are two distinct possibilities to define the lateral dimension of the sample volume. First, if a specific hotspot was giving rise to the signal, long bursts should be observed as the particle moves over a tiny excitation volume. Alternatively, if the SERS signal is either delocalized or arising from multiple hotspots, the effective lateral area should correlate with the laser spot size. The short signal duration observed, similarity of autocorrelation decays from particles of the same size on separate SERS substrates, and our previous work showing a uniform SERS and dark-field scattering intensities on the diffraction-limited length scale[18] supports the latter scenario. Figure 3B shows that when the axial height is fixed at 5 nm, the measured diffusion constant increases with respect to the axial radius.

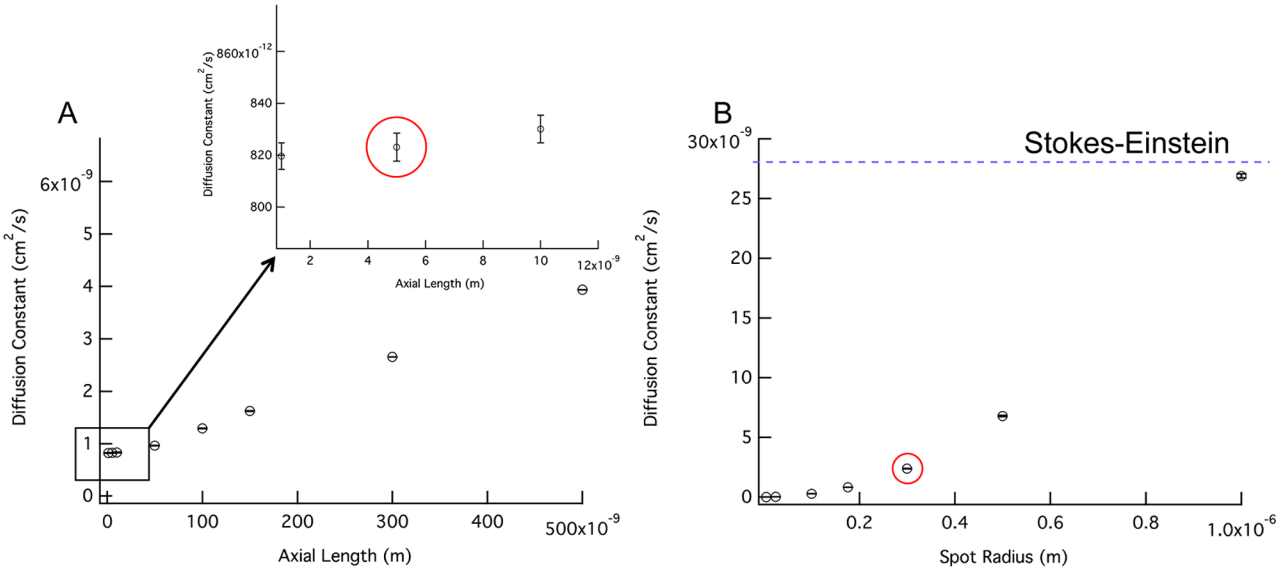

Figure 3. The average diffusion constants calculated from a set of 150 nm DPPC vesicle autocorrelation curves are plotted as a function of focal volume fit parameters. (A) The average diffusion constant as a function of the axial dimension with the radial dimension held constant at 176 nm. The inset plot shows the physically relevant region from a = 1−10 nm. (B) The average diffusion constant as a function of the laser spot radius (r) with the axial component (a) held constant at 5 nm. The blue line in B represents the calculated Stokes−Einstein diffusion constant based on the particle radius as determined by DLS. The red circles in the plots represent the fit parameters used for the calculation of diffusion constants for the whole of the data presented (r = 176 nm and z = 5 nm).

dx.doi.org/10.1021/ac403882h | *Anal. Chem.* 2014, 86, 2625−2632

Figure 1D shows autocorrelated traces for each of the frequencies shown in Figure 1C. Again, a model for three-dimensional Brownian motion was fit to the autocorrected curves to determine the autocorrelation decay time (eq 2) and diffusion constant via eq 3. The fitting results are shown as dashed lines. Representative decay times are determined by averaging all decay time values determined from the intensity profiles that satisfy the Pearson's r threshold, with the standard deviation serving as the error. When the axial height (a) is approximated to be the extension of the SERS field into solution (5 nm), the fits shown for each of the aforementioned frequencies corresponds to an average correlation decay time of 180 ± 99 ms.

Particles sizes were independently measured using dynamic light scattering. PS beads with reported diameters of 1100, 300, and 100 nm were found to have diameters of 890 ± 150, 440 ± 42, and 110 ± 10 nm, corresponding to diffusion constants calculated from eq 4 on the order of 10^{-8}–10^{-9} cm^2/s.

The average SERCS correlation decay time of 180 ± 99 ms for the 440 nm diameter PS beads in Figure 1 corresponds to a diffusion coefficient of 4.27 ± 0.076 × 10^{-10} cm^2/s (eq 3). The measured diffusion constant is an order of magnitude slower than expected based on Stokes–Einstein diffusion.

SERCS results were obtained for three PS bead samples, and the diffusion coefficients determined by SERCS and calculated from eq 3 are 1.10 ± 0.39 × 10^{-10}, 4.98 ± 0.10 × 10^{-10}, and 5.49 ± 0.12 × 10^{-10} cm^2/s, respectively. These diffusion coefficients represent the average value from all frequencies satisfying the specified Pearson's r criterion (n = 24–39). For each particle size, the diffusion constant calculated from eq 4 using the particles size determined by DLS (10^{-8}–10^{-9} cm^2/s) is an order of magnitude faster than the average diffusion constant determined by SERCS (10^{-10} cm^2/s). These results indicate that all sizes of PS particles are experiencing hindered diffusion at the SERS surface.

DPPC Vesicles. Single-shell unilamellar vesicles (SUVs) provide a means to verify how far the SERS enhancement extends from the surface. SUVs are commonly used as models for lipid and cellular membranes.[32] The structure of a lipid vesicle with hydrophobic headgroups on the exterior, a hydrocarbon layer of approximately 4–5 nm between opposing headgroups, and a solution filled center provide additional insight regarding the effective SERS penetration depth in our sampling volume.

Figure 4 shows a representative kinetic series of 500 spectra with 175 nm DPPC vesicles collected at 31 Hz (25 ms acquisitions). Figure 4A shows the changes in the SERS spectrum with respect to time. The inset spectrum shows a comparison between a reference DPPC Raman spectrum and the SERS spectrum at t = 12.54 s. Intensities at 713, 1065, 1098, and 1298 cm^{-1} indicate the presence of a DPPC vesicle in the enhancing region. These frequencies can be assigned to the choline (713 cm^{-1}), carbon–carbon (1065 cm^{-1}), and phosphate stretches (1098 cm^{-1}), and the C–H twist (1298 cm^{-1}) modes of DPPC.[33,34] These vibrational modes are consistent with the functional groups present in the head groups of DPPC molecule, which are situated on the periphery of the vesicle. The headgroup dominant spectrum supports the assertion that the extension of the SERS field into solution is limited to a finite (<5 nm) length, which is effectively where SERS no longer provides significant enhancement.

Lipid vesicles extruded through polycarbonate membranes were found to have diameters of 750 ± 35, 580 ± 220, 170 ± 31, 150 ± 51 via DLS. Figure 4, panel B demonstrates the measurable difference in autocorrelation curves observed with different size particles using SERCS. Autocorrelated 1095 cm^{-1} intensity traces for four DPPC vesicle sizes 750 (red), 580 (orange), 170 (green), and 150 nm (blue) are shown as dashed lines. The fit of eq 2 to the data, with an approximation of the axial height (a) to be SERS field extension of 5 nm, are shown as solid lines corresponding to decay times of 1100 ± 180, 500 ± 100, 160 ± 23, and 82 ± 17 ms, which correlate to diffusion coefficients of 7.3 ± 1.4 × 10^{-11}, 1.54 ± 0.08 × 10^{-10}, 4.92 ± 0.02 × 10^{-10}, and 9.43 ± 0.01 × 10^{-10} cm^2/s. Similarly to PS, the calculated diffusion constants for DPPC are slower than predicted by Stokes–Einstein diffusion. In addition, the data demonstrate a measurable difference in the diffusion constant for different size particles, as determined via SERCS.

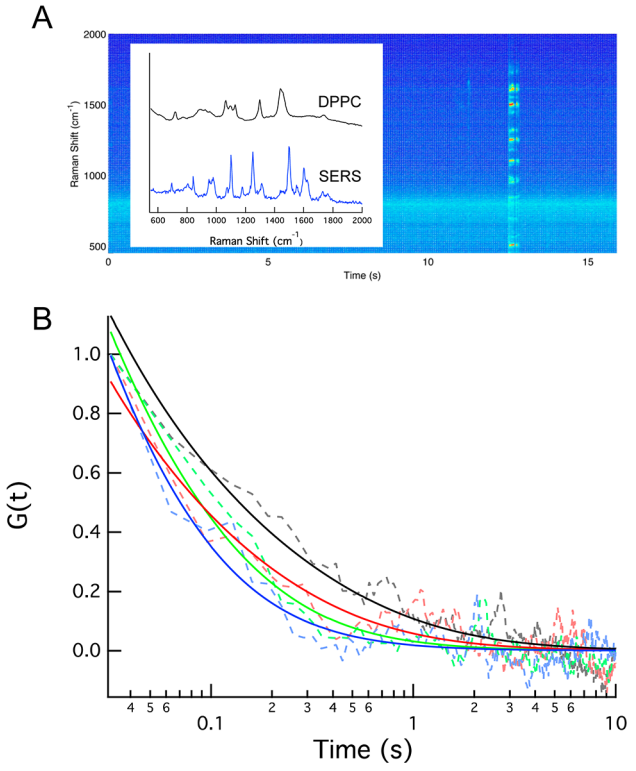

Figure 4. Sample heat map and spectrum (inset) for correlation analysis of DPPC vesicles (A). The inset spectra show a comparison of a DPPC reference to the spectrum at t = 12.54 s. Panel B shows a comparison of autocorrelation intensity curves at 1095 cm-1 and fits from vesicles of four diameters: 750 (black), 580 (red), 170 (green), and 150 nm (blue).

In addition to the headgroup dominant spectrum observed for DPPC, the limited SERS decay length can be further corroborated by the intensity of the spectral data observed. The number of oscillators sampled should increase with the extent of the SERS enhancing field and, thus, improve the signal-to-noise ratio from particles interacting in this region. Shown in Figure 5 is the measured signal-to-noise ratio as a function of bead or vesicle radius. For PS beads, the average signal-to-noise was calculated from profiles at 1009 cm^{-1} whereas 1065 cm^{-1} was used for DPPC vesicles. The standard deviations from these averages are represented as error bars. Contrary to the expected trend, the observed signal-to-noise ratio decreases as particle radius increases. The average signal-to-noise ratios for DPPC vesicles with radii of 76, 87, 292, and 377 nm were measured to be 13 ± 3, 8 ± 2, 7 ± 2 and 7 ± 1. The decrease in

dx.doi.org/10.1021/ac403882h | Anal. Chem. 2014, 86, 2625–2632

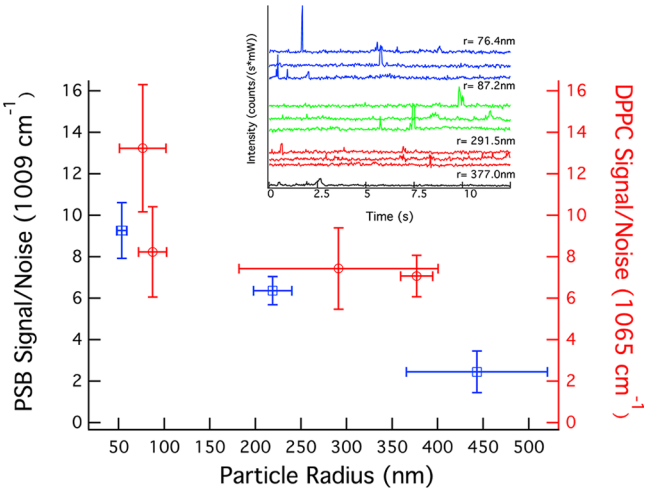

Figure 5. Plot of measured signal-to-noise ratios for PS beads (blue) and DPPC vesicles (red) at 1009 and 1065 cm-1, respectively, as a function of particle radius. Inset plot shows sample profiles for DPPC of four particle radii: 377 (black), 292 (red), 87 (green), and 76 nm (blue).

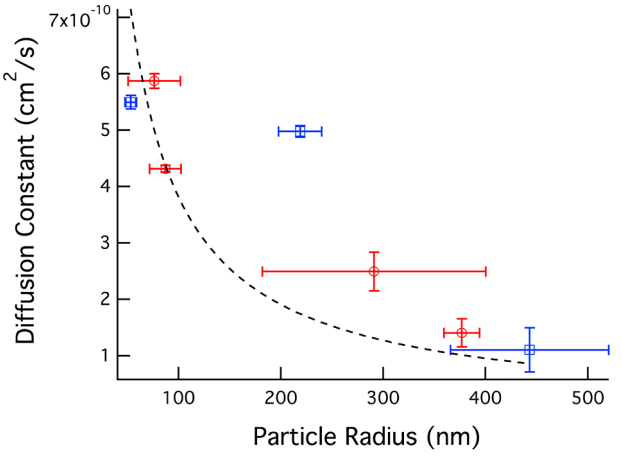

Figure 6. Plot of the average measured diffusion constant vs particle size for PS beads (blue) and DPPC vesicles (red) with an axial height (a) of 5 nm. The dotted line shows a $1/r$ function fit to the aggregated data.

intensity can be explained by increased Rayleigh scattering of the excitation laser by larger particles, decreasing the incident laser power onto the SERS surface. This diminished incident power decreases the local electric field strength that gives rise to the SERS signal as well as the probability of observing a particle.

Since the surface area of a spherical cap of a defined height scales linearly with particle radius, the negligible increase in signal with larger particle indicates the SERS signal must arise from a very small height, on the order of 5 nm (or less), as used in our analysis. The decrease in power from Rayleigh scattering is expected to be small; however, it appears to be the dominant effect as the change in SERS signal with increased surface area, or correspondingly number of molecules, is negligible. The scattering of the incident radiation also imposes a concentration limit to which this analysis can be applied. Only sufficiently dilute, or homogeneous solutions, can be analyzed via this reflection geometry.

The combined results from multiple measurements on different substrates and the determination of particle diffusion coefficients are shown in Figure 6. The coefficients were calculated on the basis of decay times from multiple spectral frequencies using the confined sensing volume (height = 5 nm) characteristic of SERS. The blue squares show results for PS beads the red circles for DPPC vesicles. A trend line for the combined data set show that, as expected on the basis of eq 4, the measured diffusion constant trends as $1/r$ with respect to particle radius. On average, the observed SERCS diffusion constants are at least 40 times slower than those predicted by Stokes–Einstein diffusion.

DISCUSSION

The results presented above indicate that SERCS can be used to gain information about analytes interacting with the SERS substrate. From the parameters measured, the relative size of the interacting particle can be assessed, but also, the absorptive interactions with the surface can be monitored.

Particle Sizing and Surface Diffusion Measurements. Correlation analysis is commonly used to determine the size of particles based on Stokes–Einstein diffusion. Although SERCS offers advantages over previous reports of correlation spectroscopy utilizing Raman spectroscopy, its utility for absolute particle sizing is debatable. The signal enhancement provided by the SERS substrate allows for collection of entire SERS spectra on the order of milliseconds, enabling selectivity between multiple species by distinguishing between the analyte in question and contaminants. The qualitative difference in the signals from different size particles is demonstrated in Figures 4 and 6; however, our results indicate that Stokes–Einstein diffusion is not observed on SERS substrates. Qualitative changes associated with particle size are observed, but the interactions at the surface inhibit the use of eq 4 for determining quantitative particle sizes or diffusion constants. Absent of prior knowledge of the particle sizes in this study, determination of size would be difficult, if not impossible; however relative changes in diffusion associated with size can be addressed.

SERCS has other advantages for monitoring diffusion. The ability to perform cross-correlation analysis allows us to statistically determine which modes exhibit the same temporal behavior and can thus be attributed to a single species. This addition decreases the error associated with the measurements. Further, the laser powers used in this study are an order of magnitude less than those reported for RCS,[24] lessening perturbation, a benefit when this methodology is applied to photo- or temperature-sensitive systems.

The range of accessible particle sizes that can be interrogated with substrate-based SERCS is limited by two factors: First, the lower limit is tied to the readout time of the EMCCD camera. Particles or molecules that diffuse through the signal generation volume faster than the minimum read time are problematic. Second, the elastic light scattering of particles increases with both size and concentrations. Our results above suggest the upper limit of particle size analysis is related to the wavelength of light used for measurements and, thus, the extent of scattering, as shown in Figure 5. As presented, the range of concentrations that can be interrogated is also limited. If the particle or vesicle concentration is to small, the probability of a particle having a fruitful interaction with the surface is decreased, leading to a poor sampling statistics. Conversely, if the particle concentration is too large, scattering of both the

dx.doi.org/10.1021/ac403882h | Anal. Chem. 2014, 86, 2625–2632

excitation and scattered light by particles in solution decreases the probability of observing signal.

Implications for SERS Detection. The observed SERS signals indicate that the enhancement does not extend more than a few nanometers from the SERS substrate. The headgroup dominated DPPC SERS spectra in Figure 4 and changes in signal-to-noise with particle size in Figure 5 support the assertion that the SERS enhancement is highly confined to the substrate surface. It is interesting to note that the signal fluctuations detected all suggest impeded diffusion at the surface. Previous reports on the penetration depth of SERS used reporter groups attached at fixed distances from the surface.[20,21] In our study, the particles are free to diffuse away, yet the signals observed suggest the SERS signal arises from particles that show a favorable, adsorptive, interaction at the surface.

The size of the particles detected requires the signals observed to originate from extra-hot spot enhancements. The signal enhancements observed from rhodamine molecules on nanoparticle aggregates support the existence of such enhancements.[16] In addition, calculations by Schatz show that an oscillating dipole outside of the gap region can evince a large scattered field.[35] Molecular absorption was reported to increase SERS limits of detection for analytes in flowing solutions.[36] The hindered diffusion associated with SERCS detection suggests physisorption or other interactions to the SERS substrate. Because the particles detected are all too large to fit into nanogaps, our results suggest these extra-hotspot enhancements may require molecules to be in physical contact with or confined within a couple nanometers of the nanostructures.

The observation of significant SERS beyond hotspots suggests extended utility for chemical sensing. Our results suggest that the enhanced Raman scattering arises from molecules adsorbed or confined near the enhancing nanostructured surface. It is known that finite element calculations fail at distances less than 1 nm from the surface.[37] Thus, molecules adsorbing to the surface may experience larger than predicted enhancements.

CONCLUSIONS

Surface enhanced Raman spectroscopy has been utilized to facilitate rapid spectral acquisition from 30 to 80 Hz. When combined with auto- and cross-correlation analysis, rapid spectral acquisition affords the ability to monitor and measure interactions between 100 and 1000 nm diameter particles diffusing in solution and a planar SERS substrate. Measurements of particle diffusion constants show that detected particles are experiencing hindered diffusion at the surface, suggesting that the observed SERS signals arise from a physical interaction between the particles and the SERS substrate. This method provides a chemically specific means of monitoring surface interactions and dynamics on chemically and biochemically relevant time scales.

AUTHOR INFORMATION

Corresponding Author

*E-mail: Schultz.41@nd.edu.

Notes

The authors declare no competing financial interest.

ACKNOWLEDGMENTS

The authors acknowledge support through a Cottrell Scholar Award from Research Corporation for Science Advancement, NIH award R21 GM107893, and the University of Notre Dame.

REFERENCES

(1) McNay, G.; Eustace, D.; Smith, W. E.; Faulds, K.; Graham, D. *Appl. Spectrosc.* **2011**, *65* (8), 825−837.
(2) Stiles, P. L.; Dieringer, J. A.; Shah, N. C.; Van Duyne, R. R. *Annu. Rev. Anal. Chem.* **2008**, *1*, 601−626.
(3) Kneipp, K.; Kneipp, H.; Kneipp, J. *Acc. Chem. Res.* **2006**, *39* (7), 443−450.
(4) Fleischmann, M.; Hendra, P. J.; McQuillan, A. J. *Chem. Phys. Lett.* **1974**, *26* (2), 163−166.
(5) Jeanmaire, D. L.; Vanduyne, R. P. *J. Electroanal. Chem.* **1977**, *84* (1), 1−20.
(6) Moskovits, M. *Rev. Mod. Phys.* **1985**, *57* (3), 783−826.
(7) Camden, J. P.; Dieringer, J. A.; Zhao, J.; Van Duyne, R. P. *Acc. Chem. Res.* **2008**, *41* (12), 1653−1661.
(8) Blackie, E. J.; Le Ru, E. C.; Etchegoin, P. G. *J. Am. Chem. Soc.* **2009**, *131* (40), 14466−14472.
(9) Michaels, A. M.; Jiang, J.; Brus, L. *J. Phys. Chem. B* **2000**, *104* (50), 11965−11971.
(10) Kneipp, K.; Wang, Y.; Kneipp, H.; Perelman, L. T.; Itzkan, I.; Dasari, R.; Feld, M. S. *Phys. Rev. Lett.* **1997**, *78* (9), 1667−1670.
(11) Nie, S.; Emory, S. R. *Science* **1997**, *275* (5303), 1102−1106.
(12) Campion, A.; Kambhampati, P. *Chem. Soc. Rev.* **1998**, *27*, 241−250.
(13) Jiang, J.; Bosnick, K.; Maillard, M.; Brus, L. *J. Phys. Chem. B* **2003**, *107* (37), 9964−9972.
(14) Fang, Y.; Seong, N.-H.; Dlott, D. D. *Science* **2008**, *321* (5887), 388−392.
(15) Wustholz, K. L.; Henry, A.-I.; McMahon, J. M.; Freeman, R. G.; Valley, N.; Piotti, M. E.; Natan, M. J.; Schatz, G. C.; Duyne, R. P. V. *J. Am. Chem. Soc.* **2010**, *132* (31), 10903−10910.
(16) Willets, K. A.; Stranahan, S. M.; Weber, M. L. *J. Phys. Chem. Lett.* **2012**, *3* (10), 1286−1294.
(17) Asiala, S. M.; Schultz, Z. D. *Chem. Commun.* **2013**, *49* (39), 4340−4342.
(18) Asiala, S. M.; Schultz, Z. D. *Analyst* **2011**, *136* (21), 4472−4479.
(19) Nishijima, Y.; Khurgin, J. B.; Rosa, L.; Fujiwara, H.; Juodkazis, S. *Opt. Expr.* **2013**, *21* (11), 13502−14.
(20) Dieringer, J. A.; McFarland, A. D.; Shah, N. C.; Stuart, D. A.; Whitney, A. V.; Yonzon, C. R.; Young, M. A.; Zhang, X. Y.; Van Duyne, R. P. *Faraday Discuss.* **2006**, *132*, 9−26.
(21) Lal, S.; Grady, N. K.; Goodrich, G. P.; Halas, N. J. *Nano Lett.* **2006**, *6* (10), 2338−2343.
(22) Frisken, B. J. *Appl. Opt.* **2001**, *40* (24), 4087−4091.
(23) Haustein, E.; Schwille, P. *Annu. Rev. Biophys. Biomol. Struct.* **2007**, *36*, 151−169.
(24) Schrof, W.; Klingler, J. F.; Rozouvan, S.; Horn, D. *Phys. Rev. E* **1998**, *57* (3), R2523−R2526.
(25) Laurence, T. A.; Braun, G.; Talley, C.; Schwartzberg, A.; Moskovits, M.; Reich, N.; Huser, T. *J. Am. Chem. Soc.* **2009**, *131* (1), 162−169.
(26) Laurence, T. A.; Braun, G. B.; Reich, N. O.; Moskovits, M. *Nano Lett.* **2012**, *12* (6), 2912−2917.
(27) Punj, D.; Mivelle, M.; Moparthi, S. B.; van Zanten, T. S.; Rigneault, H.; van Hulst, N. F.; Garcia-Parajo, M. F.; Wenger, J. *Nat. Nanotechnol.* **2013**, *8* (7), 512−6.
(28) Marr, J. M.; Li, F.; Petlick, A. R.; Schafer, R.; Hwang, C. T.; Chabot, A.; Ruggiero, S. T.; Tanner, C. E.; Schultz, Z. D. *Langmuir* **2012**, *28* (32), 11883−11889.
(29) Kellar, E. J. C.; Galiotis, C.; Andrews, E. H. *Macromolecules* **1996**, *29* (10), 3515−3520.
(30) Rodgers, J. L.; Nicewander, W. A. *Am. Stat.* **1988**, *42* (1), 59−66.

(31) Elson, E. L.; Magde, D. *Biopolymers* **1974**, *13* (1), 1−27.
(32) Chan, Y. H. M.; Boxer, S. G. *Curr. Opin. Chem. Biol.* **2007**, *11* (6), 581−587.
(33) Schultz, Z. D.; Levin, I. W. *Annu. Rev. Anal. Chem.* **2011**, *4* (1), 343−366.
(34) Spiker, R. C., Jr.; Levin, I. W. *Biochim. Biophys. Acta* **1975**, *388* (3), 361−73.
(35) Ausman, L. K.; Schatz, G. C. *J. Chem. Phys.* **2009**, *131* (8), 10.
(36) Negri, P.; Jacobs, K. T.; Dada, O. O.; Schultz, Z. D. *Anal. Chem.* **2013**, *85*, 10159−10166.
(37) Esteban, R.; Borisov, A. G.; Nordlander, P.; Aizpurua, J. *Nat. Commun.* **2012**, 3.